Far-infrared Rydberg-Rydberg transitions in a magnetic field:
Deexcitation of antihydrogen atoms

A. Wetzels, A. Gürtler, and L. D. Noordam

FOM Institute for Atomic and Molecular Physics, Kruislaan 407, 1098 SJ Amsterdam, The Netherlands

F. Robicheaux

Department of Physics, Auburn University, Auburn, Alabama 36849, USA
(Received 6 January 2006; published 16 June 2006)

The dynamics of (de)excitation between highly excited Rydberg states ($15 < n < 60$ of Rb) in a magnetic field of 0.85 ± 0.05 T is studied with far-infrared pulses (90–110 and 50 μm) originating from a free electron laser. We measured the excitation spectrum to states around $n = 40$ from a deeper bound state near $n = 25$. Moreover, starting from a highly excited state ($30 < n < 60$) below and in the n-mixing regime we investigated the efficiency of the deexcitation channel vs the ionization channel. We measured deexcitation efficiencies well above 50% for some of the states. However, starting deep in the n-mixing regime the deexcitation efficiency is less than 10%. The measurements were in good agreement with fully quantum mechanical calculations. Calculations for deexcitation of $n = 35$ states in H found the largest amount of deexcitation for $m = 0$ and almost none for $m = 20$. In recent experiments at CERN, antihydrogen is produced in high n states in a strong magnetic field with a wide distribution of m. Our measurements and calculations suggest that deexcitation stimulated by infrared photons is not an efficient method for accelerating cascade to the ground state.

PACS number(s): 36.10.−k, 32.60.+i, 32.30.Bv, 32.80.Rm

I. INTRODUCTION

Since the discovery of quasi-Landau resonances in barium [1,2] there has been strong interest in the behavior of Rydberg atoms in strong magnetic fields. The experiments [3,4] of Rydberg atoms in a magnetic field were accompanied by extensive theoretical calculations. In the beginning the theoretical work was restricted to the hydrogen atom [5–7] because of its "simplicity," but later calculations also were done for a multi-electron system such as helium [8,9]. The hydrogenic ℓ-m degeneracy of the n manifolds of the Rydberg series is lifted by the magnetic field. In a strong field, the manifolds of adjacent n states intersect. This is known as the n-mixing regime ($n > 43$ for 0.85 T). Most of the previous measurements and calculations were for ground, or nearly ground, initial states. Here we study the transitions *between* highly excited states $n \to n'$. We investigated both the excitation ($n' > n$) and deexcitation ($n' < n$) behavior. Experimental and theoretical studies of transitions from $n = 10$ states in Li [10,11] and a more general theoretical treatment [12] have been performed for strong magnetic fields but weak laser fields, where the population transfer is very small. The present experiments and calculations are not directly comparable to this work because we are interested in stronger laser intensities where the competition between excitation and deexcitation is important.

The deexcitation behavior is particularly interesting for accelerating the radiative cascade of antihydrogen to the ground state. Recently, antihydrogen atoms (consisting of a positron bound to an antiproton) have been generated in Rydberg states in the presence of a strong magnetic field [13,14]. Measurements [15] and calculations [16] showed that the generated antihydrogen atoms occupy highly excited Rydberg states ($n \geq 50$). To make precision tests of how an atom of antimatter might differ from its ordinary-matter counterpart, the antihydrogen atom has to be in the ground state. How the positrons have to decay to the ground state is an open question. Presumably, it will decay by radiative cascade because it spends the majority of its time in vacuum even though radiative cascade in a strong magnetic field can be much slower than for the field-free case [17,18].

We investigated the possibility of using laser deexcitation to drive the antihydrogen more rapidly to lower n levels. One can envision two alternative deexcitation paths (see Fig. 1). Path 1: starting in the n-mixing regime the atom can be deexcited by one photon transition towards a Rydberg state below the n-mixing regime ($\Rightarrow$ a). A second laser could then be used to deexcite the atom further ($\Rightarrow$ b) until radiative
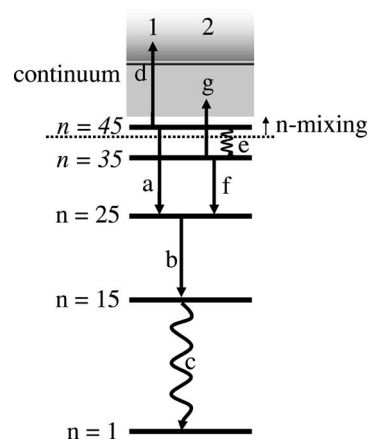

FIG. 1. In this figure two different possible pathways are shown for the deexcitation of antihydrogen towards the ground state. In path 1 laser deexcitation can be used as the first step, in path 2 the (antihydrogen) atom first has to be deexcited below the n-mixing regime with another method (e.g., collisions) before laser deexcitation can be used.
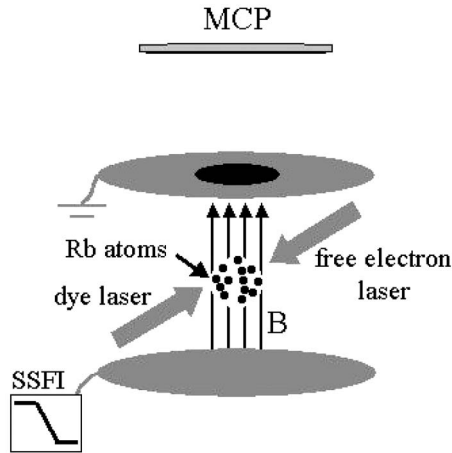
FIG. 2. In a magnetic field of 0.85 (±0.05) T rubidium atoms are excited with a dye laser system to a Rydberg state. Hereafter a far infrared photon (de-)excites the atom further. The final state distribution is measured with state selective field ionization by ramping a negative voltage on the lower plate.

decay becomes efficient enough to deexcite the atom to the ground state (⟹ c) [19]. During laser deexcitation electrons can be lost via the competitive ionization channel (⟹ d). Alternatively in path 2 the atoms are first deexcited to a Rydberg state below the n-mixing regime by collisional deexcitation (e^-+Atom $n=45 \Rightarrow e^-$+Atom $n=35$) (⟹ e). Once the atom is below the n-mixing regime laser deexcitation can be used to deexcite the atom further (⟹ f and b) until radiative decay can deexcite the atom towards the ground state (⟹ c). Again a fraction of the electrons will be lost by the competitive ionization channel (⟹ g). In the experiment reported here we compare the deexcitation efficiency starting from a Rydberg state *below* and *in* the n-mixing regime (⟹ a vs f) and the competition between the deexcitation and ionization channel (⟹ a and f vs ⟹ d and g).

In Sec. II we will describe the experimental setup. We performed spectroscopy starting in low lying rubidium Rydberg states ($28s$, $29s$ and $27d$) and excited higher lying Rydberg states around $n=40$ to determine the transition efficiency between different angular momentum states (Sec. III). Next we measured the deexcitation vs ionization efficiency as a function of the wavelength and intensity of the free electron laser starting from different highly excited states, below and above the n-mixing regime (Sec. IV). We investigated the effect of the laser pulse width on the fraction of atoms that were ionized (Sec. V). We performed calculations for many of the experimental cases and for Rydberg states of H (Sec. VI).

II. EXPERIMENTAL SETUP

A schematic drawing of the experimental setup is shown in Fig. 2. The experiment is performed in an electron spectrometer developed by Kruit and Read [20] in which an inhomogeneous magnetic field was used to direct the electrons towards the detector. The magnetic field strength in the interaction region is 0.85 (±0.05) T. Inside the electron spec-

trometer rubidium was evaporated in a resistively heated oven. Rydberg atoms are created by nonresonant two-photon excitation of ground-state rubidium atoms using a Nd:yttrium–aluminum–garnet pumped dye laser. After this, the Rydberg atoms were illuminated with far infrared light from the free electron laser (FELIX) in Rijnhuizen, the Netherlands [21].

The free electron laser produces picosecond long (6–20 ps) far infrared pulses separated by an interval of 40 ns. These short micropulses form a train, the macropulse, with a length up to 6 μs. The macropulses have a repetition rate of 5 Hz. A pulse slicing system cuts a few micropulses out of the macropulse with an exponential decaying intensity. The far infrared beam is focused to a spot size of 3 mm^2 by a parabolic mirror with $f=20$ cm into the reaction region. Because of the presence of water absorption lines in the scanning region, the far infrared beam was transported through a system of vacuum tubes to the electron spectrometer.

The final distribution of the Rydberg atoms after exposure to the far infrared radiation (initial state population, excitation or ionization and deexcitation yield) was determined by state selective field ionization (SSFI) [22,23]. The electric field was ramped in time such that the higher Rydberg states would ionize earlier than the lower Rydberg states. Ejected electrons of Rydberg atoms were driven to the microchannel plate detector by a small static electric field.

III. EXCITATION

In Fig. 3 the results of a spectroscopy measurement are shown. The initial state, respectively $28s$, $29s$ [Fig. 3(a)] and $27d$ [Fig. 3(b)], is excited with a far infrared photon (90–110 μm) to final states near the n-mixing regime. We indicated the position of the p and f states for a field-free situation in Fig. 3. In a one-photon transition the population in the s state will be excited towards a p state. In Fig. 3(a) the excited p states are shifted 0.8 cm^{-1} compared with a field-free situation due to the diamagnetic shift, which is 0.8 cm^{-1} for a p state near $n=40$ in a magnetic field of 0.8 T [22]. Starting in a d state [Fig. 3(b)] both ap state and f state can be excited in a one-photon transition. According to the Bethe rule a $\Delta \ell=+1$ transition is favored over the $\Delta \ell=-1$ transition in hydrogen. However, Fig. 3(b) shows that the opposite is the case for rubidium. Theoretical calculations in absence of a magnetic field [24] show also that excitation from the d state to a higher-lying state does not obey the Bethe rule, and that indeed d-p transitions are more likely than d-f transitions. In both graphs [3(a) and 3(b)] we see a dip in the excitation spectrum (indicated by the circle). This dip is caused by deexcitation towards a lower state instead of excitation to a higher-lying Rydberg state. In the case of an initial d state, deexcitation towards an f state is favored above deexcitation towards a p state as predicted by theory [24].

In Fig. 4 the Zeeman states near $n=42$ and $n=43$ are plotted as a function of the magnetic field. In a magnetic field the ℓ-m degeneracy of the Rydberg states is lifted by the field. In a strong magnetic field the manifolds of adjacent n
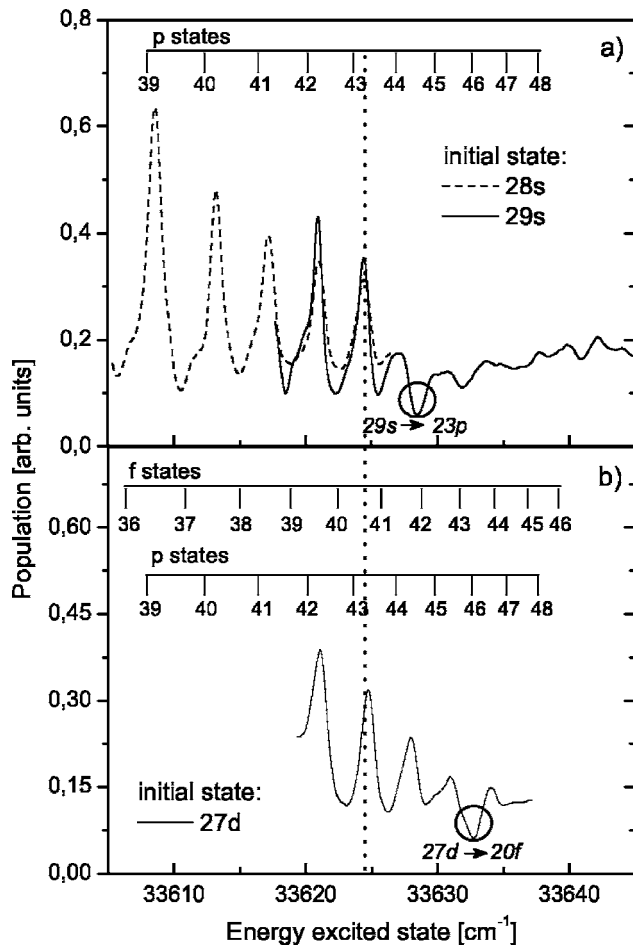
FIG. 3. Excitation spectrum around the n-mixing regime starting from (a) 28s, 29s and (b) 27d. The spectrum was obtained by scanning the frequency of the far infrared laser so that the same region of final state energy was reached from each of the initial states.

states intersect. The calculated Zeeman spectrum shows that this n-mixing regime in a magnetic field of 0.9 T starts between $n=42$ and $n=43$. This agrees nicely with the measurement where the peak structure cannot be resolved near 45p situated in between the $n=42$ and $n=43$ manifolds.

IV. DEEXCITATION

Deexcitation and ionization (excitation) are two competing channels during photon interaction of Rydberg atoms. In this experiment we compare the efficiency of the deexcitation channel vs the ionization channel to find the most favorable circumstances for deexcitation of Rydberg states. We compare initial states above and below the n-mixing regime (respectively routes 1 and 2 in Fig. 1). The ionization and deexcitation behavior of $n=35d$ (below n mixing) as a function of the wavelength is shown in Fig. 5. We scanned the far infrared photon from 90 to 110 μm, so that we covered the deexcitation region between $n=23$ and $n=24$. As expected, ionization does not depend strongly on the wavelength. Deexcitation, however, only happens when the photon transition is on resonance. In the case of rubidium the cross section to
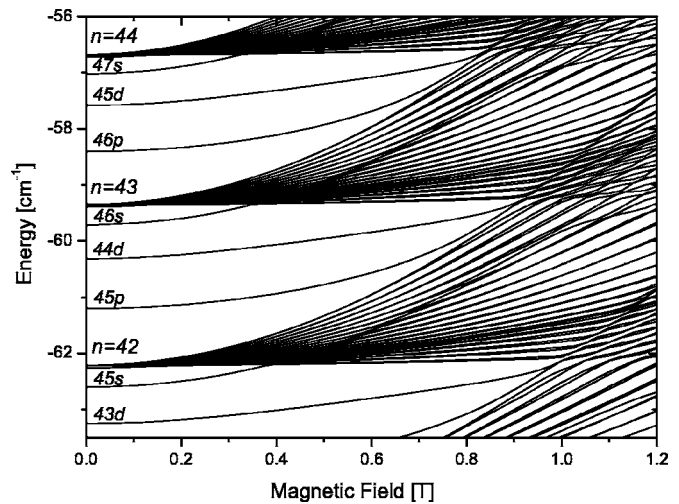

FIG. 4. Zeeman spectrum of $m=0$ Rydberg states near $n=42$ and $n=43$. The calculations did not include spin-orbit coupling.

the p state is negligible and only deexcitation to 23f and 24f is observed. In the inset of Fig. 5, two scans of the deexcitation from 35d to 24f are shown at two different peak intensities of the free electron laser. The deexcitation yield changes as the peak intensity varies but the resonance width does not change in our intensity range. The full width at half maximum (FWHM) of the deexcitation peak is 1.4 cm^{-1} and is not limited by the bandwidth of the free electron laser (FWHM=0.65 cm^{-1}). The quantum calculations do not exhibit this behavior for the linewidth and we do not have a good explanation for it at this time.

The next step is to set the far infrared light on a deexcitation resonance near 100 μm and scan the intensity of the free electron laser. We investigated the response for several combinations of initial states and deexcited resonance states. In Fig. 6, the initial state population, deexcitation and ionization yield are shown as a function of the intensity for different initial states, respectively 30d, 35d below the
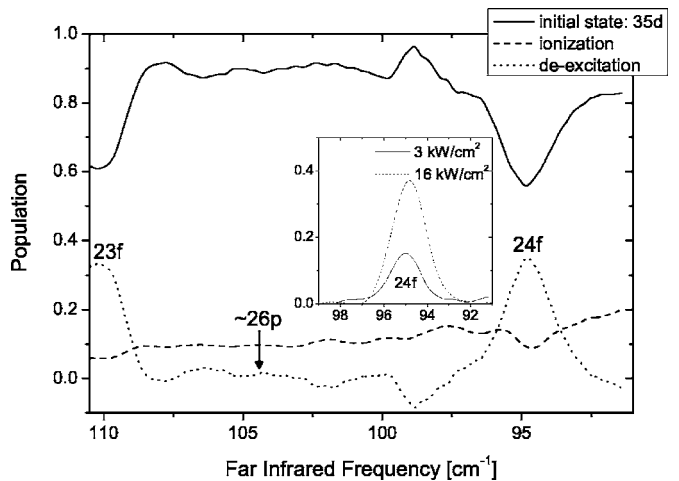

FIG. 5. The population of the initial state, deexcitation and ionization efficiency are measured while the wavelength of the far infrared photon is scanned. In the inset the deexcitation is shown for two different intensities with a pulse duration of ~20 ps.
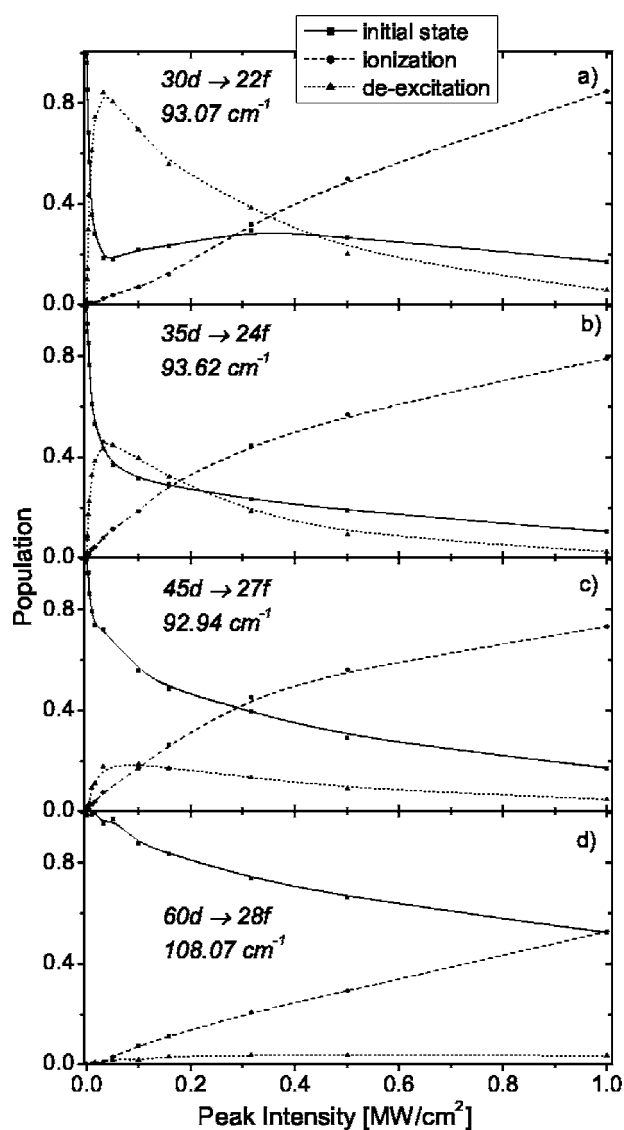
FIG. 6. The population of the initial state, deexcitation and ionization probability are measured as a function of the intensity of the free electron laser for different initial states below and in the n-mixing regime.
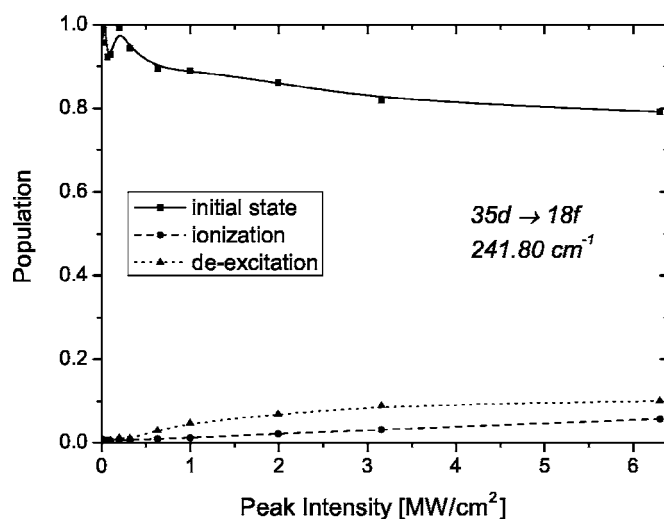

FIG. 7. The population of the initial state, deexcitation and ionization probability are measured as a function of the intensity of the free electron laser. The wavelength of the far infrared photon is set around 40 μm.

the far infrared photon for this measurement. Although the ionization channel is not efficient, because we excite a state far in the continuum, the deexcitation is not efficient either. The initial and final state are too far separated so that the overlap between the two states is too small. We conclude that transitions between nearby-lying states at low frequencies are favored over high-frequency transitions.

V. INFLUENCE OF LASER BANDWIDTH AND PULSE TRAIN ON IONIZATION PROBABILITY

The free electron laser pulse contains a few micropulses separated by 40 ns which decrease exponentially in intensity. This 40 ns separation makes it possible to detect the ionization yield per micropulse on the digital oscilloscope. In Fig. 8, the ionization probability per pulse is measured as a function of the intensity of the free electron laser. One initial state below the n-mixing threshold is chosen [$35d$ in Figs. 8(c) and 8(d)] and one initial state in the n-mixing regime [$45d$ in Figs. 8(c) and 8(d)]. This experiment is performed for two different bandwidths, respectively, for 0.65 cm^{-1} [Figs. 8(a) and 8(c)] and 2.0 cm^{-1} [Figs. 8(b) and 8(d)] to show the influence of the pulse duration on the ionization probability. The results show that the ionization by the longer pulse is more efficient than by the shorter pulse. Our quantum calculations gave the same ionization fraction for the same fluence of the short and long laser pulse as long as the laser intensity was low. At larger laser intensities, the calculations found more ionization for the longer pulse although the effect was not large. For the most part, the ionization fraction decreases with successive micropulses due to depletion of the initial state and decreasing intensity; we do not have a simple explanation for the exception [micropulses 1 and 2 in panel (d)].

VI. THEORY

Our calculations for this system were fully quantum mechanical, but we did not include the spin-orbit effect which is

n-mixing threshold and $45d$, $60d$ in the n-mixing regime. On-resonance photon deexcitation works rather well. We observed deexcitation yields higher than 50%. The intensity of the far infrared light is important for the deexcitation yield. If the intensity is too low no deexcitation is observed because the transition rate is too low. If the intensity is too high, all of the atoms are ionized, including the initially deexcited atoms. Comparing the different initial states we see that deexcitation is more efficient if the initial state is below the n-mixing threshold. Just above the n-mixing threshold [Fig. 6(c)], the deexcitation efficiency is still 20%. But far into the n-mixing regime [Fig. 6(d)], as in the antihydrogen experiment, almost no deexcitation signal is observed. We repeated the experiment with a shorter wavelength. Starting from the $35d$ state we tried to deexcite the population with a $\sim$40 μm photon to the $18f$ state. In Fig. 7 the deexcitation and ionization probability are shown as a function of the intensity of
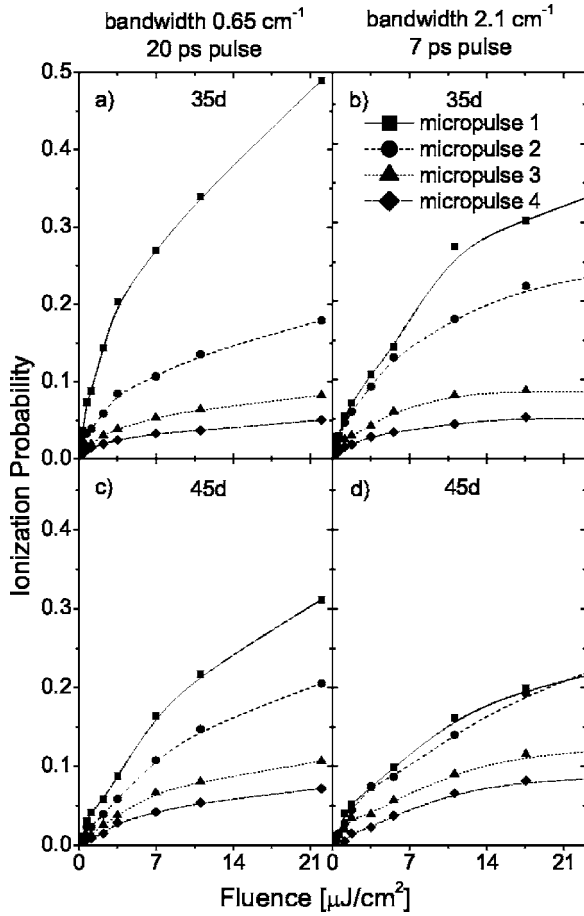
FIG. 8. The ionization per free electron laser pulse is shown as a function of the intensity. The intensity ratio of the micropulses is $1:0.5:0.38:0.25$. The experiment is performed at two different initial states, below and in the n-mixing regime, and at two different bandwidths to show the influence of the pulse duration on the ionization yield.

negligible for the resolution of the experiment. The calculations were performed by representing the wave function through an expansion in spherical coordinates

$$\Psi(r_j,\theta,\phi,t) = \sum_\ell R_\ell(r_j,t)Y_{\ell m}(\theta,\phi)/r_j, \qquad (1)$$

where the time dependent radial functions are only known on a grid of points. We chose the radial grid points to be a square root mesh where $r_j=s_j^2$ with $s_j=j\Delta s$; this scaling is very effective for Rydberg states which have nodes with approximately equal spacing in s. The radial derivatives were performed using a Numerov-like method (see the appendix of Ref. [25]) which gives high order accuracy but only couples the radial point r_j to $r_{j\pm1}$. The polarization of the laser field and the direction of the magnetic field were both taken to be in the z direction which means m is a conserved quantum number. The two fields couple together the angular momenta; the laser couples ℓ to $\ell\pm1$ and the magnetic field couples ℓ to $\ell\pm2$ which means the combination of the two fields gives a penta-diagonal structure to the field part of the Hamiltonian. Because of the low frequency, we compute the

laser-atom interaction using the length gauge. There are three angular matrix elements that are important

$$C_{\ell\ell'} \equiv \langle \ell m|\cos\theta|\ell'm\rangle = \sqrt{\frac{\ell_>^2 - m^2}{(2\ell+1)(2\ell'+1)}}\,\delta_{|\ell-\ell'|,1} \qquad (2)$$

for the laser atom interaction,

$$\langle \ell m|\sin^2\theta|\ell m\rangle = 1 - C_{\ell,\ell+1}^2 - C_{\ell,\ell-1}^2 \qquad (3)$$

for the diagonal term of the magnetic field potential, and

$$\langle \ell-1,m|\sin^2\theta|\ell+1,m\rangle = -C_{\ell-1,\ell}C_{\ell,\ell+1} \qquad (4)$$

for the off-diagonal term of the magnetic field potential.

The field-free atomic potential was chosen to have the form of a model potential

$$V_\ell(r) = -\frac{1}{r}(1 + [Z-1]e^{-\beta_\ell r} + \gamma_\ell r e^{-\lambda_\ell r})$$

$$-\frac{\alpha}{2r^4}(1 - \exp[-r^3])^2, \qquad (5)$$

where Z is the charge of the nucleus, α is the polarizability of the ion (0 for H and 9.076 for Rb$^+$), and β_ℓ, γ_ℓ and λ_ℓ are fit parameters that give experimental quantum defects for the Rydberg states. For H, all of the constants are 0. For Rb, β_ℓ is 4.123 99, 4.286 52, and 4.004 91, γ_ℓ is 9.061 34, 9.677 57, and 9.177 43, and λ_ℓ is 1.714 29, 1.741 85, and 1.815 71; for all constants, the numbers are for s, p, and d waves with the constants for $\ell>2$ equal to those for $\ell=2$. Convergence was checked with respect to the number of radial grid points and the number of angular momenta by increasing these parameters until the final result was unchanged. Typically, we used up to $\ell=90$ and 2500 radial mesh points in a spherical box of 6000 a.u.

The solution of the time dependent Schrödinger equation must utilize an implicit method due to the stiffness of the equations and the long times involved (roughly 10^7 atomic units or more). The method we used can be derived in two steps. We first note that the atomic Hamiltonian only couples together adjacent points in r (from the kinetic energy operator) but does not affect ℓ, whereas the field part of the Hamiltonian does not change r but couples together the ℓ. Since the action of each Hamiltonian is separately easy to account for, we use a split operator method

$$\Psi(t+\delta t) = \exp(-iH_1\delta t/2)\exp(-iH_2\delta t)\exp(-iH_1\delta t/2)\Psi(t)$$

$$+ O(\delta t^3), \qquad (6)$$

where $H=H_1+H_2$ and the H_1,H_2 are at the time $t+\delta t/2$ if they contain time dependence. We evaluated the exponentials using a fifth order Padé approximation that exactly preserves the unitarity for Hermitian Hamiltonians

$$\exp(-ix) = \left(\frac{1-iax}{1+iax}\right)\left(\frac{1-ia^*x}{1+ia^*x}\right) + O(x^5), \qquad (7)$$

where $a=(1+i/\sqrt{3})/4$; these equations can be solved efficiently using standard linear algebra packages due to the sparse nature of our representation of the Hamiltonian opera-

tors. This approximation to the exponential is somewhat dangerous because the phase error when $x \gg 1$ causes very high energy states to appear to have low energy. Thus it is important to test convergence with δt to make sure the propagator is not giving spurious results. In all of the calculations, we used δt less than 1/800 of the Rydberg period of the initial state, $2\pi\nu^3$.

Finally, we need to be able to compute the fraction of the wave function that absorbed a photon, the fraction that remained in the initial state, and the fraction that was deexcited. In the experiment, this was accomplished by measuring when the atom was ionized in relation to a ramping electric field. This calculation could be done but it would be very time consuming. Instead, we used an inward moving radial mask to distinguish these states. For example, the Rb $35d$ state has a binding energy of approximately 96.5 cm^{-1} and we expose it to photons with an energy of 93.6 cm^{-1}. The part of the wave function corresponding to excitation reaches much larger r while the deexcitation part of the wave function only extends to 1/2 the radial size. By slowly moving in the mask (over 50 ps), we can completely remove one part of the wave function before the mask starts affecting the other parts.

In the calculation, we only have one laser pulse interact with the atom, unlike the experiment which has several pulses. Unless stated otherwise, the laser pulse in the calculation has the Gaussian shape $E_{max}\cos(\omega t)\exp(-t^2/t_w^2)$ where t_w is 8 ps. For this choice of t_w, the bandwidth of the laser is 1.56 cm^{-1} FWHM which is larger than the experimental width (0.65 cm^{-1}) by a little more than a factor of 2. We did not try to exactly match the experimental parameters because propagating the wave function between laser pulses would have dramatically slowed the calculation. In all that follows, we do not expect to get perfect agreement between calculation and experiment but the general trends should be similar.

A. Results for Rb

In Fig. 9, we show the computed excitation spectrum starting from the $28s$, $29s$, and $27d$ states. A comparison with Fig. 3 shows that there is a good agreement between measurement and calculation. In particular, notice that the dips due to deexcitation are in good agreement. The dips are present because the laser intensity is strong. For weak intensities, there is no dip in the excitation spectrum because there is no depletion of the initial state due to deexcitation.

In Fig. 10, we show the population of different levels when the atom starts in the $35d$ state which has a binding energy of 96.5 cm^{-1}. There is good agreement with the measurement in Fig. 5. In particular, notice that the population that is deexcited can greatly exceed the fraction ionized when the laser is tuned to a resonance. It may seem that the ionization fraction is not affected by the resonances but this is because the ionization fraction is much less than 1 so variations are not obvious. At both of the large resonances, the ionization fraction dips by approximately 10%. Again, the dips in the ionization are because the laser is strong and the initial state is depleted due to deexcitation. The peak near 110 cm^{-1} corresponds to transition to the $23f$ state while the
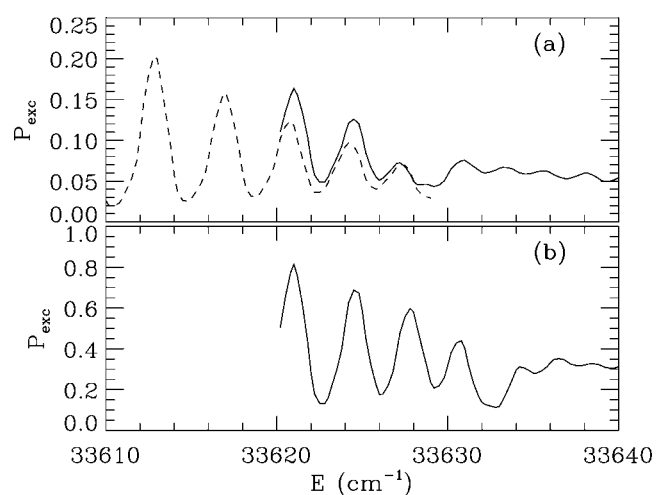

FIG. 9. Excitation spectrum around the *n*-mixing threshold starting from (a) $28s$ (dashed line), $29s$ (solid line) and (b) $27d$. Compare to Fig. 3. As in the experiment, the $29s$ and $27d$ spectra show dips corresponding to deexcitation.

transition near 95 cm^{-1} is to the $24f$ state. The deexcitation probability is stronger to the $24f$ because the dipole matrix element is larger. The ionization probability decreases with increasing photon energy. Both trends are due to the fact that the dipole matrix elements are largest for smaller energy transitions. There are weak deexcitation peaks near 88 and 105 cm^{-1} which correspond to *p* states.

We next examined the dependence of the ionization fraction compared to deexcitation from different initial states. In Fig. 11, we show the calculation for the resonant transitions $30d \rightarrow 22f$ and $35d \rightarrow 24f$ which should be compared to the measurements in Fig. 6. Again, the agreement between the measurements and calculations is very good considering the different laser properties. For these states, the deexcitation probability rises much more rapidly than the ionization probability so there is an intensity where the atom can be driven to lower energy with high efficiency. However, the ionization probability becomes increasingly important at higher intensities. The calculations show a weak, but clear, oscillation in
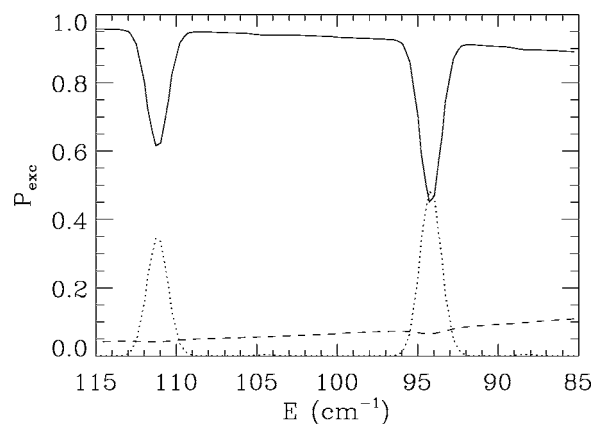

FIG. 10. The calculated population of the initial state (solid), deexcitation (dotted) and ionization (dashed) efficiency are plotted vs the energy of the far infrared photon. The laser intensity was chosen to be 16 kW/cm^2. Compare to Fig. 5.
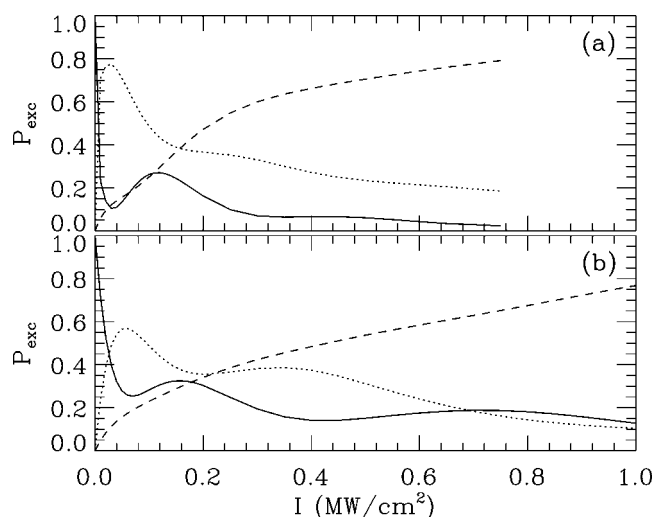
FIG. 11. The calculated population of the initial state (solid), deexcitation (dotted) and ionization (dashed) efficiency are plotted vs the peak intensity of the laser field. In (a), the initial state is the $30d$ and the laser has an energy of 93.07 cm^{-1} which gives a resonant transition to the $22f$ state. In (b), the initial state is the $35d$ and the laser has an energy of 93.62 cm^{-1} which gives a resonant transition to the $24f$ state. Compare to Fig. 6.

the probabilities of finding the atom in the excited state vs the deexcited state. This is due to the Rabi oscillation of a strongly driven two-level system. This effect is not seen in the experiment, probably because the multiple laser pulses add a level of decoherence which destroys the oscillation. Finally, Fig. 11 does not show curves for $45d$ and $60d$ initial states. We performed calculations for the $45d$ state and found behavior completely different from that seen in Fig. 6(c). The results of the calculations did not look physically reasonable even though the calculations appeared to be converged. This is because the calculation is for an initial state which is a Rydberg wave packet since many levels exist within our excitation of d character near the $45d$ energy level. While this is an interesting system, it is not relevant for our current investigations.

B. Results for H

Since part of our motivation was to explore methods for accelerating the radiative cascade in the anti-hydrogen experiments, we performed calculations in H. Hydrogen is an experimentally more difficult system to work with although there is no extra difficulty for the calculation. The main difference between Rb and H is that the initial state in the calculation was a single state for Rb, whereas the ℓ states are mixed by the magnetic field for H. Therefore, it is not obvious which state to take as the initial state. In all of our calculations, we took states within the $n=35$ manifold with either $m=0$, 10, or 20. For each of the m's, we made the initial state by photoexciting the $\ell=m$ character of the state with a laser pulse of width $t_w=8$ ps. This gives a wave packet in which the components of different ℓ oscillate for constant m. For each m, we examined two different deexcitation times: one where the peak of the second laser pulse was 96 ps after
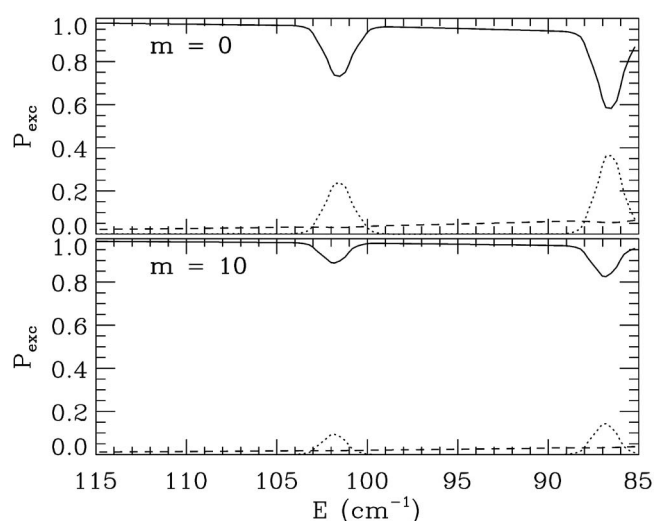

FIG. 12. The calculated population of the initial state (solid), deexcitation (dotted) and ionization (dashed) efficiency are plotted vs the energy of the far infrared photon for $n=35$ wave packet with $m=0$ and with $m=10$. The laser intensity was chosen to be 16 kW/cm^2. Compare to Figs. 5 and 10 for Rb.

the peak of the pulse that made the wave packet and the second where the peak of the second laser pulse was 196 ps after the peak of the pulse that made the wave packet. While there were clear differences between the two different times for deexcitation, the results were qualitatively the same. We will only present results for the deexcitation pulse 96 ps after the pulse that formed the $n=35$ wave packet.

In Fig. 12, we show the population of different levels when the atom starts in the $n=35$ wave packet described above. These curves are qualitatively the same as Figs. 5 and 10 for Rb. The resonance at 87 cm^{-1} is for deexcitation to $n=25$ states and the resonance at 102 cm^{-1} is for deexcitation to $n=24$. As with Rb, the deexcitation can greatly exceed the ionization fraction on resonance. However, the $m=10$ deexcitation fraction is much less than the $m=0$ fraction. We also performed calculations for $m=20$ but there was very little photon absorption or emission at this intensity. This can be understood because the $m=10$ (and especially the $m=20$) states have less probability to be at smaller distances where photon absorption and emission occurs.

We next examined the dependence of the ionization fraction compared to deexcitation from different initial states. In Fig. 13, we show the calculation for the resonant transitions $n=35 \rightarrow 24$ for the $m=0$ wave packet and the $m=10$ wave packet. These should be compared with the Rb curve (b) in Figs. 6 and 11. We have not shown the $m=20$ curves because they do not show interesting features; the ionization and deexcitation fraction increase roughly linearly with ionization of 6.4% and deexcitation of 2.2% at the highest intensity. As with the calculation for Rb, there is some Rabi oscillation between the initial n and the deexcited n. There is also a region where the deexcitation fraction is larger than the ionization fraction for each of the m's. However, the peaks of the deexcitation population are not at the same intensity. This illustrates another difficulty in trying to accelerate the cascade of antihydrogen by laser deexcitation. The antihydrogen
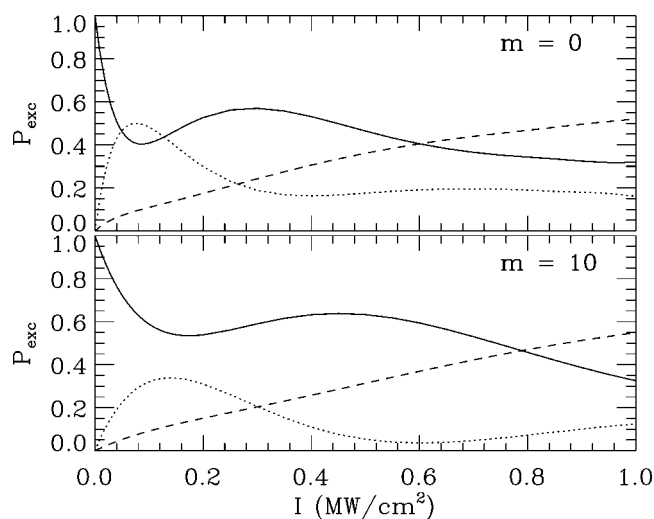
FIG. 13. The calculated population of the initial state (solid), deexcitation (dotted) and ionization (dashed) efficiency are plotted vs the peak intensity of the laser field for $n=35$ wave packet with $m=0$ and with $m=10$. The photon energy was chosen to be 101.6 cm^{-1} to be resonant with deexcitation to $n=24$. Compare to Figs. 6 and 11 for Rb.

will be in a large range of m which means the laser will be able to efficiently deexcite only a fraction of the population.

VII. CONCLUSION

We have experimentally and theoretically investigated the possibility for laser stimulated deexcitation of atoms when ionization is a competing channel. To deexcite the electron the photon energy has to be on resonance. In the case of

deexciting Rb, our measured and calculated results suggest that laser deexcitation becomes efficient for low-ℓ states below the n-mixing regime. Transitions between nearby-lying states are favored over high-frequency transitions. Low intensity of the deexcitation laser is preferred, or else the deexcited electron will be excited again and finally ionize. Our results suggest that laser deexcitation will not be effective unless collisional deexcitation drives the atom below the n-mixing threshold; unfortunately, the short interaction times of the antihydrogen with the positron plasma may not allow this to occur [16].

Unfortunately, the magnetic field mixes the ℓ states for H because the quantum defects are 0 which means the efficiency is not as high as for Rb. Furthermore, the antihydrogen will be made in a range of m values and the higher m do not respond to laser fields as well as the low m. Therefore, it seems that laser stimulated deexcitation is not a promising method for accelerating the radiative cascade of antihydrogen.

[1] W. R. S. Garton and F. S. Tomkins, Astrophys. J. **158**, 839 (1969).

[2] R. J. Fonck, D. H. Tracy, D. C. Wright, and F. S. Tomkins, Phys. Rev. Lett. **40**, 1366 (1978).

[3] J. Neukammer, H. Rinneberg, K. Vietzke, A. König, H. Hieronymus, M. Kohl, H.-J. Grabka, and G. Wunner, Phys. Rev. Lett. **59**, 2947 (1987).

[4] G. R. Welch, M. M. Kash, C.-H. Iu, L. Hsu, and D. Kleppner, Phys. Rev. Lett. **62**, 893 (1996).

[5] A. Holle, J. Main, G. Wiebusch, H. Rottke, and K. H. Welge, Phys. Rev. Lett. **61**, 161 (1988).

[6] M. L. Du and J. B. Delos, Phys. Rev. A **38**, 1896 (1988a).

[7] M. L. Du and J. B. Delos, Phys. Rev. A **38**, 1913 (1988b).

[8] B. Hüpper, J. Main, and G. Wunner, Phys. Rev. Lett. **74**, 2650 (1995).

[9] B. Hüpper, J. Main, and G. Wunner, Phys. Rev. A **53**, 744 (1996).

[10] N. Bouloufa, P. Cacciani, D. Delande, C. Delsart, J. C. Gay, E. Luc-Koenig, and J. Pinard, J. Phys. II **2**, 671 (1992).

[11] N. Bouloufa, P. Cacciani, D. Delande, C. Delsart, J. C. Gay, E. Luc-Koenig, and J. Pinard, J. Phys. B **28**, L755 (1995).

[12] P. A. Braun and D. Delande, J. Phys. B **27**, 5621 (1994).

[13] M. Amoretti *et al.*, Nature (London) **419**, 456 (2002).

[14] G. Gabrielse *et al.*, Phys. Rev. Lett. **89**, 213401 (2002).

[15] G. Gabrielse *et al.*, Phys. Rev. Lett. **89**, 233401 (2002).

[16] F. Robicheaux, Phys. Rev. A **70**, 022510 (2004).

[17] J. R. Guest, J.-H. Choi, and G. Raithel, Phys. Rev. A **68**, 022509 (2003).

[18] T. Topcu and F. Robicheaux, Phys. Rev. A **73**, 043405 (2006).

[19] E. S. Chang, Phys. Rev. A **31**, 495 (1985).

[20] P. Kruit and F. H. Read, J. Phys. E **16**, 313 (1983).

[21] D. Oepts, A. van der Meer, and P. van Amersfoort, Infrared Phys. Technol. **36**, 297 (1995).

[22] T. F. Gallagher, *Rydberg Atoms* (Cambridge University Press, Cambridge, 1994).

[23] F. Robicheaux, C. Wesdorp, and L. D. Noordam, Phys. Rev. A **62**, 043404 (2000).

[24] J. H. Hoogenraad and L. D. Noordam, Phys. Rev. A **57**, 4533 (1998).

[25] F. Robicheaux, J. Phys. B **29**, 779 (1996).